Fragments of matter from a maximum-entropy viewpoint

1991 J. Phys.: Condens. Matter 3 1019

(http://iopscience.iop.org/0953-8984/3/9/001)

J. Phys.: Condens. Matter 3 (1991) 1019–1053. Printed in the UK

REVIEW ARTICLE

Fragments of matter from a maximum-entropy viewpoint

R Englman
Soreq Nuclear Research Centre, Yavne 70600, Israel

Received 30 July 1990

Abstract. After introducing the formalism of maximum entropy and reviewing alternative approaches for fragment size statistics, this paper derives a general distribution law (similar in form to the Bose–Einstein statistics) and applies it to distributions observed in rock mining, exploding metallic shells, shattered crystal pieces, droplets in spray, atomic or molecular clusters, space debris and fragmented nuclei. Variations of fragment number with size that are power-law-like (fractal), humped or exponential can lead to physically significant conclusions regarding the fracturing mechanism. Theoretical aspects of the maximum-entropy method in the derivation of the distribution law (including some inherent difficulties) are discussed.

1. Introduction

The pieces of a broken object are among the most common examples of randomness and disorder (Zurek 1989, section V). There may be psychological reasons for associating disorder with broken pieces, perhaps due to our dismay at seeing a nicely designed object shattered and to the need to clean up the resulting mess, but it is a fact that it has been found difficult to read some regularity into fragments. The regularity that we can hope to get is a law describing the *distribution* of fragments, especially with respect to their sizes but also regarding shapes and internal parameters. The prediction of distribution has in many cases practical advantages, relevant to scientific and technological issues. A few instances taken from physics will be given later (section 6); at this point I shall describe the industrial importance of oil-shale fragment size distribution since it was through this that I became involved in fragmentation.

In a standard mode of operation (called 'bench blasting') the bituminous rock (oil shale) is explosively mined to produce the debris containing fragments. The large specimens are then comminuted mechanically to bring them down to a size such that retorting (or extraction of oil by partial burning) can be carried out. Since comminution takes time and money, large fragments (exceeding about 50 cm in diameter) are undesirable, and so are small pieces (less than 0.5 cm) since these clog up the retort. The mining has to be planned accordingly and, while one rarely has control over the geomechanical properties (faults, cracks, etc) of the rock, one can still vary some parameters of the mining, namely, location of explosion boreholes, temporal sequence of their activation and type of explosive. By correct choice of these one can hope to obtain a fragment size distribution with the desired properties of not having too many pieces

0953-8984/91/091019 + 35 $03.50

outside the lower and upper limits. The task at hand is thus the derivation of a fragment size distribution in the context of a physical process (the passage of detonation stress waves) and in a given geometric setting (some borehole pattern and major fault structure in the rock) (Jaeger *et al* 1986b). At the same time, several physical factors will remain unknown, like subsurface joints and cracks, leaving the theoretician with an underdefined assignment.

It would appear that the maximum-entropy method (MEM) is an ideal tool to handle this situation and others in which we wish to predict fragment distributions. Reasons both favouring and opposing this expectation are outlined in the next section and in appendix 1, where we return to a discussion on the claims of MEM.

Fracture of solids as a physical process is the subject of appendix 2.

2. The method of entropy maximization

Let us denote by j the events that we wish to predict (like the event of finding n fragments of a given size in a debris heap) and by p_j the corresponding probabilities. We then assert that the MEM gives the most conservative probability distribution p_j subject to the available knowledge, which enters the formalism as 'constraints'. The maximum-entropy solution is that which maximizes the information entropy (also called 'missing information')

$$S = -\sum_j p_j \log p_j \tag{1}$$

(Shannon 1948) subject to the constraints. The constraints are assured mathematically by Lagrange multipliers (appendix 1).

The meaning of 'most conservative' in the assertion of the last paragraph is twofold. First, the MEM probabilities p_j are about the smoothest, flattest functions of the events j (suitably ordered) consistent with the constraints; secondly, the predictions p_j make do with just the constraints explicitly imposed and not with any other constraints perhaps tacitly implied (in obtaining non-MEM p_j). The latter meaning provides a simple, heuristic proof of the assertion. It can be shown that imposing any additional constraints reduces S, i.e. it reduces the 'missing information'. If our choice for the probabilities p_j is non-MEM, this choice will reduce S below its maximum value and will imply some extra constraint. Therefore the MEM solution is the only one consistent with the explicitly stated knowledge.

More impressive claims have also been made for the MEM as a predictive method (Jaynes 1983, Skilling 1984, Rosenblatt-Roth 1987, 1988). In the context of fragmentation, one can show that, if N independent fragmentation experiments are performed, the mean of the size distributions will tend, asymptotically as $N \to \infty$, to the MEM value of p_j.

A consistency criterion was enunciated by Tikochinsky *et al* (1984) in the following sense: the distribution of MEM is the only one that will be confirmed by successive repetition of experiments.

In view of the existence of several time-honoured and practised predictive procedures (like maximum-likelihood, least-squares fitting, Bayesian predictions), the preceding claim is bound to have raised opposition (Titterington 1984). To answer this, Skilling (1984) writes: 'I find the arguments for using maximum entropy to be deeply compelling. [MEM] stands in splendid isolation, on fundamental grounds.'

But even this is not all, since according to Jaynes (1983), MEM predictions *cannot* be mistaken: if they are not supported by experiment, they must be regarded as disclosing (the need for or existence of) additional informational constraints. Jaynes is to be credited with the use of information entropy as a predictive tool in physics and this review does perhaps no more than describe the implementation of this programme for fragmentation. In his works (collected in Jaynes (1983)) thermodynamic entropy is represented as a measure of the insufficiency in our knowledge of a physical system. In an opposite view (Denbigh and Denbigh 1985) thermodynamic entropy is regarded as an objective attribute of the system. In a compromise approach (Zurek 1989) the thermodynamic entropy is a sum of contributions of physical randomness and of the observer's ignorance.

Without taking sides in this controversy, we wish to demonstrate here that the maximum-entropy solution p_j with energy $\hat{E}$ given is formally identical to the minimum-energy solution P_j with entropy $\hat{S}$ given. With the introduction of Lagrange multipliers, denoted by β, ν and T, μ (respectively) for the two problems, the quantities (henceforth called Lagrangians) to be extremized are

$$L = S - \beta(E - \hat{E}) = -\sum_j p_j \log p_j - \beta\left(\sum_j \varepsilon_j p_j - \hat{E}\right) - \nu\left(\sum_i p_i - 1\right) \tag{2}$$

and

$$-\Lambda = E - T(S - \hat{S}) = \sum_j \varepsilon_j P_j + T\left(\sum_j P_j \log P_j + \hat{S}\right) - \mu\left(\sum_j P_j - 1\right). \tag{3}$$

The sets of equations $\partial L/\partial p_j = 0$ and $\partial \Lambda/\partial P_j = 0$ have evidently formally the same solutions. These become equal,

$$p_j = P_j = \exp(-\varepsilon_j/T) \Big/ \sum_i \exp(-\varepsilon_i/T) \tag{4}$$

if one supposes the relations

$$T = \beta^{-1} = \hat{E}/\hat{S}. \tag{5}$$

Clearly equation (4) is also the solution obtained by minimizing the free-energy expression (for temperature T given). The maximum-entropy procedure would thus appear to be beyond doubt, but questions remain whether the system (especially a classical one) is truly ergodic over the events j.

3. Distribution of fragments

3.1. Exponential distributions based on MEM

Apparently the earliest use of MEM for fragment size distribution is due to Griffith (1943). He supposed that:

(i) a given quantity of energy is converted to fragmentation (this quantity depending on the nature and intensity of the fracturing process);
(ii) the energy goes entirely into the creation of free surfaces; and
(iii) each molecule in the solid competes for the available energy on equal footing.

If N_s denotes the number of molecules belonging to s-sized fragments, N_s/s is the number of s-sized fragments. The energy invested in each fragment is $\gamma s^{2/3} g$, where γ is the surface energy density and g a geometrical factor. The constraint is

$$\hat{E} = \gamma g \sum_s s^{2/3} N_s/s = \gamma g \sum_s s^{-1/3} N_s \tag{6}$$

so that identifying ϵ_j in equation (2) with $\gamma g s^{-1/3}$ and regarding the solutions in equation (4) one derives

$$N_s \propto \exp(-\lambda/s^{1/3}) \tag{7}$$

where λ is a constant to be evaluated from equation (6). In practice, in the break-up of solids, the number of fragments N_s/s decreases with size much faster than that given by equation (7), indicating that assumption (iii) places too much weight on large fragments and that sinks of energy other than the surface energy (involved in assumption (ii)) are also present. Moreover, molecules in the middle of the fragment do not feel the fracture process in the same way as do molecules on the surface. We shall see that when fragments are formed by accretion of molecules, assumption (iii) has an empirical basis (section 6.4).

In a discussion of the size distributions of exploding shells and of other two-dimensional objects, Grady and Kipp (1985) used only a geometrical constraint, namely

$$A = g \sum_s n_s s \tag{8}$$

meaning that the number n_s of plane fragments of size s times their area gs (where g is again a geometrical factor) sums up to the total area A. The MEM soution is clearly

$$n_s \propto \exp(-gs/A). \tag{9}$$

This is to be contrasted with the semiempirical distribution due to Mott (1947) (see also Mott and Linfoot 1943) in which the cumulative distribution arising from n_s is an exponential function of the *linear* size, namely $s^{1/2}$ in two dimensions and $s^{1/3}$ in three dimensions. Data on metallic shells have been accounted for by Mott's distribution (Sternberg 1973), though discrepancies appear, which are treated in greater detail in section 6.1. Deviations from Mott's law have been found in fragmented rock data and in a numerical simulation (Englman *et al* 1984).

3.2. Fragmentation by a fast, sudden process

Fracture by fast energy input, such as occurs in explosions, projectile or laser impact, a shattering event, explosive expansion or a sharp temperature change, has been the subject of dynamic theories (Mott 1947, Grady 1982, Grady *et al* 1985, Glenn and Chudnovsky 1986, Glenn *et al* 1986, Curran *et al* 1987).

These theories are incorporated in the probabilistic prediction of fragmentation that we describe now. Characteristic of fast processes is that fracture events take place at different points of the solid independent of one another. This is because newly created fractures have no time to communicate with each other, except that the energy invested in the fracture cannot exceed the total energy available for fracture and that the fragmented volumes are also bounded by the original volume. Following Grady (1982), we suppose that all discontinuities formed by the stress wave (e.g. cracks, voids) immediately become faces of fragments. An alternative view, which remains to be explored, would

be to suppose that in the first place the fast process creates fractures that can then join up to enclose a fragment. The advantage of this second view is that unfinished fractures, called 'internal damage' (Jaeger *et al* 1986a, c, Yatom and Ruppin 1989) are also envisaged to be present as the result of stress.

Following a more detailed account in the original paper (Englman *et al* 1988b) we associate with each fragment of linear size a an energy $e(a)$ (see equation (10) below) which in essence contains all the physics entering the formation of fragments (figure 1). Summing $e(a)$ over all fragments, we equate the sum to the total energy input $\hat{E}$ for the fragmentation process: this provides the first constraint (equation (15) below). Implicit in this procedure is the assumption that at the instant of fragmentation all secondary features of the process (such as heat, noise, fragment motion) still reside in the fragments. Our way of invoking energy conservation differs from that of Glenn *et al* (1986), who balance the created surface energy against the kinetic and stored energies. The present approach appears justified (barring the role of expanding gases formed in an explosion) because it includes the physical state of the fragments immediately after fragmentation.

We assume fragments of linear size a and roughly spherical shape whose energy

$$e(a) = (2\pi/3)\rho u^2 a^3 + (2\pi/5)\rho\dot{\varepsilon}^2 a^5 + (4\pi/6K)\sigma^2 a^3 + 4\pi\gamma a^2(1 - a/R) \tag{10}$$

consists of the following terms: the kinetic energy (KE) of the fragment of mass density ρ moving as a rigid body with speed u (this term takes up the largest part of the energy); the internal KE about the centre of mass (expressed in terms of $\dot{\varepsilon}^2$, the volumetric dilatation rate squared, or the trace of the square of the stretching tensor); the stress energy stored in the fragments (Glenn *et al* 1986) including sound and elastic waves (σ being the stress and K the bulk modulus); and the surface formation energy (γ is the surface energy density and R is the radius of the spherical solid before fragmentation). Other terms depending on size a or on other variables (e.g. shape or chemical composition) may be added to equation (10).

The probability of having n_a fragments of size a is written

$$p(n_a, a) \qquad \text{with} \qquad \sum_{n_a} p(n_a, a) = 1 \tag{11}$$

and the most likely number of such fragments and their masses are, respectively,

$$\langle n_a \rangle = \sum_{n_a} n_a p(n_a, a) \tag{12}$$

and

$$w(a) = (4\pi/3)\rho a^3 \langle n_a \rangle. \tag{13}$$

Assuming that a fixed mass $\hat{W}$ of materials is being fragmented, we have the constraints

$$W = \sum_a w(a) = \hat{W} \tag{14}$$

and

$$E = \sum_a e(a)\langle n_a \rangle = \hat{E} \tag{15}$$

where the second constraint is due to energy conservation.

(In equation (11), we have chosen as the fundamental event whose probability $p(n_a, a)$ is sought the finding of n_a fragments of linear size a, rather than the event of finding

at random an a-sized fragment, whose relative frequency is $p(a)$. Our choice reflects the practice in mineral processing of the operation of sieving.)

In the sense of the MEM, the best distribution p subject to the constraints is obtained by maximizing

$$L = -\sum_a \sum_{n_a} p(n_a, a) \log p(n_a, a) - \beta(E - \hat{E}) - \mu(W - \hat{W}) \tag{16}$$

through variation of $p(n_a, a)$ and adjusting the Lagrange multipliers β and μ so that the constraints (13) and (14) are satisfied.

The solution is

$$p(n_a, a) = \exp(-n_a x_a) \Big/ \sum_{n_a} \exp(-n_a x_a) \tag{17}$$

where

$$x_a = \beta e(a) + \mu(4\pi/3)\rho a^3 \tag{18}$$

and

$$\langle n_a \rangle = (e^{x_a} - 1)^{-1} \tag{19}$$

$$\sim x_a^{-1} \tag{20}$$

for the majority of fragments, i.e. excluding large-sized fragments, for which $x_a > 1$, whose mean number decreases exponentially. In (18) the fragment mass and energy are both polynomials in a, with powers Θ ranging from 2 to 5 (equation (10)). In a size range where a single power law dominates in (18), the distribution of sizes will exhibit a power-law behaviour in the form

$$\int_a^\infty \mathrm{d}a \, \langle n_a \rangle \propto a^{-D} \tag{21}$$

with the 'fractal dimension' D being given in terms of the predominant values of Θ as $D = \Theta - 1$.

Turcotte (1986) has listed 21 objects whose fragment size distribution behaves according to (21), with D falling between 1.5 and 3.5, i.e. conforming to the theoretical values in equations (10), (18) and (20). Experiments on simulation of astroid impacts gave $D \sim 2.5$ (Capaccioni *et al* 1986).

To determine the parameters β and μ in the distribution $\langle n \rangle$ (equations (18)–(20)) from the constraints, we first combine (14) and (15) to write

$$I \equiv \beta \hat{E} + \mu \hat{W} = \sum_a x_a (e^{x_a} - 1)^{-1} \tag{22}$$

where the summation is over all sizes that are collected in discrete bins. Let the number of bins (or summands) be I_b, then

$$I < I_b \tag{23}$$

since the summand is less than unity. The dominant contribution to $e(a)$ and x_a is a term proportional to the fragment volume a^3. Thus, I is proportional to $\hat{W}$.

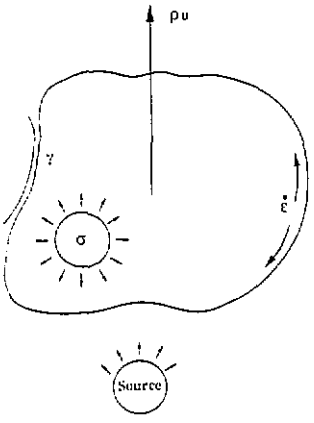

Figure 1. Forces acting on a fragment. The figure illustrates the body forces ρu (inertial) and σ (uniform stress), the surface energy density γ and the transverse dynamic strain $\dot{\varepsilon}$.

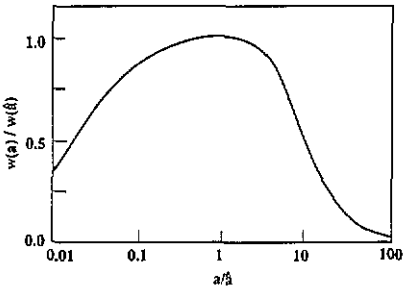

Figure 2. Weight distribution of fragments, equation (24). The weight $w(a)$ and the linear fragment size a are normalized to their values at $\hat{a}$ (equation (26)). Beyond $a/\hat{a} \sim 10^2$ the distribution drops off exponentially with a and equation (24), on which this figure is based, is not applicable. The parameter ν in equation (27) has the value 10^{-2}.

The weight distribution (13) for the majority of fragments (equation (10)) is expressed in a reduced form as

$$w(a) = \hat{W}I^{-1}/(2\nu s^{-1} + 1 + \nu s^2) \tag{24}$$

$$s = a/\hat{a}. \tag{25}$$

It has a maximum at $a = \hat{a}$, given by

$$\hat{a} = (5\gamma/\rho\dot{\varepsilon}^2)^{1/3} \tag{26}$$

which serves as a convenient scaling parameter for the fragments (Grady 1982). The other parameter ν in the distribution (24) contains the multipliers β and μ, which must be eliminated by calculating the mass (or weight) constraint (14). The result is

$$\nu = (\pi/3)(\hat{a}/Il)^2 \tag{27}$$

where l is the bin width, so that, as shown in equation (22), Il is the effective size range scanned by the sampling process. The saddle-point $\hat{a}$ must fall well inside the size range, so that

$$\nu \ll 1. \tag{28}$$

The weight distribution, shown in figure 2, has a maximum at $a = \hat{a}$, is broad, and is asymmetric. Thus, the maximum derived by MEM coincides with the characteristic fragment size of Grady (1982) and depends (through equation (26)) only on the dynamic fracture parameters γ and $\dot{\varepsilon}^2$. On the other hand, $\hat{a}$ is independent of either the centre-of-mass KE or of the stored stress σ, or indeed of any contribution to the energy that is

proportional to the fragment volume $4\pi a^3/3$. The mathematical explanation for this is that in the summand of (14),

$$w(a) \propto a^3 n_a \sim a^3 x_a^{-1} = [\beta e(a)/a^3 + \mu]^{-1}$$

all such contributions appear as an additive constant to the Lagrange multiplier μ, which is a parameter to be adjusted.

The empirical role of $\hat{a}$ is well documented in the fragmentation of oil shale (Grady 1982), brittle steel (Weiner and Rogers 1979) and rapidly heated water (Blink and Hoover 1985). Since we find that, in general, the mean size averaged over the distribution exceeds its maximum $\hat{a}$, a more careful determination of the average and a specification of the averaging procedure are called for.

In 'cratering' situations, where only part of the solid is fragmented, the constraint (14) on the total weight W does not apply and μ does not enter. Yet, remarkably, elimination of the parameter β leads to the same distribution (24) as in the fixed W situation. This was subject to test when fused alumina cement targets were partially (~30%) and almost fully (90%) fragmented by fast aluminium projectiles (Bianchi *et al* 1984). The fractal exponents were, respectively, $D = 2.76$ and 3.06, which do not support our result, though their magnitude is within the range predicted in equations (10), (18) and (20).

The weight $\hat{W}$ of the crater mass scales with the energy input $\hat{E}$ according to

$$\hat{W} = (2\pi\rho\hat{E}\hat{a}/9\gamma)(\hat{a}/l)^2. \tag{29}$$

The threshold energy input E_t below which fragmentation cannot occur (the constraint equation (15) having no solution) is given by

$$E_t = 4\pi\gamma\hat{a}^2(\hat{a}/l). \tag{30}$$

A different threshold energy for fragmentation, resulting from a geometrical constraint, was obtained by Yatom and Ruppin (1989).

A striking result of the MEM distribution is the prediction of fractal distribution, equations (17)–(20), with fractal exponents in the range of the observed ones (Turcotte 1986). The result depends on two circumstances: first, on the property that the energy and volume terms, given by $e(a)$ and a^3, go to zero as the size a vanishes so that there is no contribution to the constraints from $a \to 0$, admitting of a 'Bose condensation'; secondly, on the absence of a constraint on the total number of fragments. Since the latter circumstance is tied to the non-atomistic description, it seems that fractal distributions might be the rule for classical objects. We emphasize though that fractal, inverse power-law behaviour is predicted only for the low size end; at large sizes an exponential decrease with size takes place. In our discussion of experimental distributions in the sequel, the question of power-law versus exponential form will come up frequently.

In summary of this section, an essentially simple, two-parameter ($\hat{a}$ and ν) distribution (equation (24)) has been derived, based on the broad principle of maximum entropy and incorporating the physics of fragmentation through the energy of fragments of size a (equation (10)). The typical Grady fragment size has been rigorously rederived and identified with the saddle-point $\hat{a}$ and the maximum of the distribution; $\hat{a}$ was found to be unaffected by mechanisms that are coextensive with the fragment volume.

3.3. Statistics of propagating fragmentation

In the previous section we have described a fragmentation process that is fast, sudden and happens in space uniformly. In contrast, 'propagating fragmentation' designates a

process wherein a medium gets fragmented over an extended duration of time and in an extended volume. The 'source term' driving the fragmentation is space- and time-dependent. By maximizing the information entropy density at all times and positions, subject to constraints involving the source term, we obtain fragment size distributions that are fully determined by the source term and the strain rate. We shall find that weak (or strong) sources result in a size distribution that is sharply (or broadly) peaked around the most likely fragment size.

This is the first instance in which the duration of the fragmentation process enters our consideration. We postpone a discussion of the temporal scale of fragmentation to a later section (section 4.2) where sequential fragmentation theories are reviewed; let us note though that MEM can bear extension to processes developing in time (Jaynes 1983, p 287, Levine 1985). The present approach keeps clear of intricate issues, such as the suggestions that a perturbed system will evolve by minimal rate of entropy production not far from equilibrium and by maximal rate of entropy increase when far from equilibrium (Prigogine 1978, Kaufman *et al* 1989).

We assume that the fragmented body can be subdivided into regions of unit volume that are sufficiently large for statistical considerations to be valid in each region and at the same time small enough that external forces or stresses can be regarded as uniform throughout the region. Regions are labelled by a convenient coordinate r and the time by t. Fragments formed in (t, r) are characterized by linear size $a = a(t, r)$ where a is a parameter specifying the fragment. More generally a might represent a set of fragment parameters (size, shape, composition, quality, etc), though we shall work with a as representing exclusively the linear size of the fragment. We seek by MEM the probability

$$p(n_a, t, r) \qquad \text{with} \qquad \sum_{n_a} p(n_a, t, r) = 1 \tag{31}$$

of finding n_a fragments in unit volume around position r and at time t having the dimension a. Under the conditions posited, the total entropy of information is the sum of the entropies of the regions

$$S(t) = \sum_r S(t, r) = -\sum_r \sum_a \sum_{n_a} p(n_a, t, r) \log p(n_a, t, r). \tag{32}$$

We maximize $S(t)$ for all times, subject to constraints described in the following, to obtain first the probabilities p and then the mean fragment number per unit volume for fragments of type a,

$$\bar{n}(a, t, r) \equiv \sum_{n_a} n_a p(n_a, t, r). \tag{33}$$

The expectation value of any quantity $Q(a)$ is given by

$$\langle Q \rangle \equiv \sum_a Q(a) \bar{n}(a, t, r). \tag{34}$$

The physical foundations of the method are some theoretical or empirical relationships between the parameter of fragmentation (a) and the parameters of the physical process that causes fracture. The relations are expected to have the form

$$F(\text{fragment parameters}) = \phi(\text{stress parameters}) \tag{35}$$

of which a particular case might be

$$\langle F(a, t) \rangle = \phi(\sigma(t'), t' \leqslant t) \tag{36}$$

where on the left we take an average over a function of fragment sizes a at time t and on

the right we have a function of the history of the stress pulse σ up to the time t. Numerous forms of the functions in (36) have been considered in the past (Curran *et al* 1987, Kachanov 1986).

We shall postulate an energy balance formulation (Tuler and Butcher 1968, Kachanov 1986) equating the energy residing in the fragments with the energy input invested up to time t by the source. As already written in (15)

$$\sum_a e(a)\bar{n}(a, t, r) = \dot{E}(t, r) \tag{37}$$

where

$$\dot{E} = W \times D \tag{38}$$

$$= W \times \left(A \int_0^t [\sigma(t') - \sigma_0]^n \, dt'\right). \tag{39}$$

On the left in equation (37) is the sum over the energy density functional for fragments of size a, while on the right appears a semiempirical relation for the energy input in unit volume required to create the fragments. In (39), $\sigma(t)$ is the stress at time t and position r, σ_0 is a threshold for fracture. (In a more realistic treatment one should use several thresholds for different kinds of stresses: compressive, tensile, shear.) W is the energy at full nominal damage that specifies the energy needed to produce the damage $D = D(t)$ defined by the large parentheses. A is another empirical constant that depends primarily on the properties of the medium: its mechanical strength and its state (e.g. the population of microcracks). The power n in the integral is commonly taken as 2.

The stress $\sigma(t)$ represents the external source of fragmentation. It is regarded in this study as an input parameter, being a function of the distance from the location of the energy deposition and of time. Theoretical and empirical estimates of $\sigma(t)$ take into account the intensity of the source (e.g. the powder factor of explosives), the stress input rate and the elastic constants of the medium. The stress σ decreases oscillatorily with both t and r, due to geometry and dissipation. In truth, the energy loss due to fragment formation itself reduces σ and it is necessary to use a σ that is self-consistent with both the energy loss and the degradation of the medium. For an inhomogeneous medium (e.g. with substantial variability in crack densities inside it) A and W will also have a distance- and time-dependent behaviour.

The energy functional $e(a)$ in (37) was given in (10); we rewrite it as

$$e(a)/2\pi = \tfrac{1}{3}\rho u^2 a^3 + \tfrac{1}{3}\sigma^2 a^3/K - 2\gamma a^3/R + \varepsilon_a/2\pi \tag{40}$$

where

$$\varepsilon_a = 2\pi\dot{\varepsilon}^2 a^5/5 + 4\pi\gamma a^2. \tag{41}$$

The separation of terms in (40) distinguishes between terms with a^3 dependence and the two terms in (41) with a different variation. Since by construction we partition the fragmented material into regions of unit volume, for which following constraint holds

$$\langle a^3 \rangle = 1 \tag{42}$$

having normalized for convenience to a cubic rather than spherical volume, the expectation values of the first three terms in (40) are constant. Physically this means that the energy input for fragmentation $\dot{E}$ is fully expended on ε_a in (41), whereas the first three terms consume energy in a way that is independent of the state of fragmentation.

Maximization of (32) subject to the constraints (37) and (42) leads to the following probabilities

$$p(n_a, t, r) = \exp[-n_a(\beta\varepsilon_a - \nu a^3)] \Big/ \sum_{m_a} \exp[-m_a(\beta\varepsilon_a - \nu a^3)] \tag{43}$$

where the Lagrange multipliers β and ν serve to satisfy (37) and (42). The expected number of fragments per unit volume is, according to (33),

$$n_a = [\exp(\beta\varepsilon_a - \nu a^3) - 1]^{-1}.$$

The constraint equations give, for each form of the energy functional $e(a)$, a universally valid solution as a function of $\hat{E}$ only, i.e. independent of t and r. The physical mechanism for fragmentation enters through the dependence of $\hat{E}$ on r and t (an example for which is the integral shown in (39)).

To describe the variation of the Lagrange parameters β and ν with E we find it convenient to transform them to dimensionless form,

$$\beta' = 2\pi\gamma\hat{a}^2\beta \tag{44}$$

$$\nu' = \hat{a}^3\nu \tag{45}$$

where

$$\hat{a} = (5\gamma/\rho\dot{\varepsilon}^2)^{1/3} \tag{46}$$

is a length characteristic of fragment size (Grady 1982) shown in equation (26). With the choice of (46) for the length unit the equations determining β' and ν' are

$$1 = \langle s^3 \rangle = \sum_s s^3 n(s) \tag{47}$$

$$E' = E/2\pi\gamma a^2 = \sum_s (2s^2 + s^5) n(s) \tag{48}$$

$$n(s) = \{\exp[\beta'(2s^2 + s^5) - \nu' s^3] - 1\}^{-1}. \tag{49}$$

In these units the ratio of ε_a to a^3 is

$$\varepsilon'(s)/s^3 = 2s^{-1} + s^2. \tag{50}$$

As shown in figure 3, for $E' \to \infty$, ν' tends to the value -1.0534, while β' varies exponentially as $\exp(-1/2|\nu'|E')$. As the energy input decreases, β' increases and ν' changes sign. In the limit β' approaches infinity and ν' approaches $3\beta'$ from below. However, the limiting value of the energy E' where this occurs is not zero, but 3+, or for the physical energy in (48)

$$E \to E_{\lim} = 6\pi\gamma\hat{a}^2. \tag{51}$$

This remarkable result of an energy threshold dictated by statistical requirements, and additional to the crack-mechanical threshold implied by σ_0 in (39), will now be interpreted on the basis of equations (47)–(49). In the simplest terms, for the mean energy to be large, n has to be large, and this is tantamount to the exponent in (49) being small. Therefore β' decreases steadily with increase of energy input, as seen in figure 3. However, the increase of n has to be kept in check, since the expectation value of the volume is constant (equation (42)), and this is ensured by the other Lagrange multiplier ν' having the tendency to counterbalance the decrease of β'. More illuminating is the

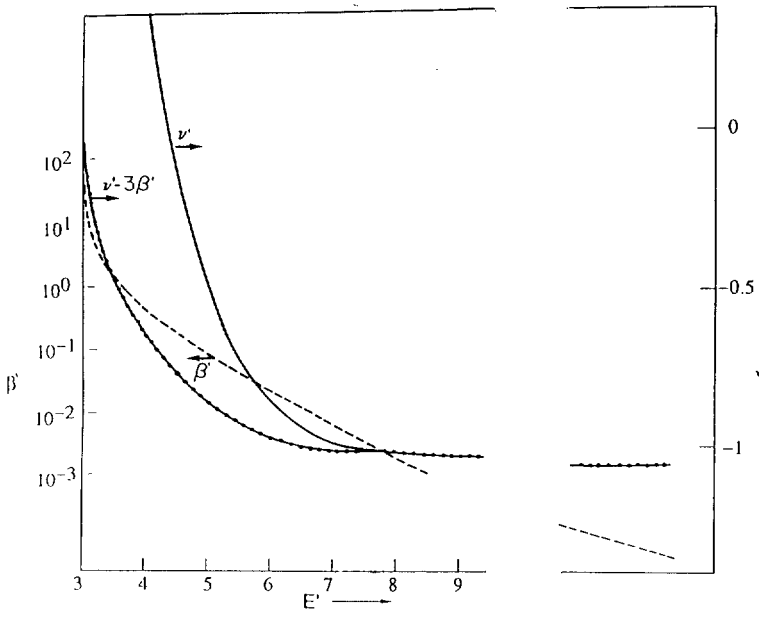

Figure 3. Lagrange multiplier parameters in the distribution as a function of the energy input E' responsible for the fragmentation. The energy multiplier β' (left-hand vertical scale) and the volume multiplier ν' and $\nu' - 3\beta'$ (right-hand scale) are shown, all in dimensionless units (equations (44), (45) and (48)). The asymptotic behaviours of β' and ν' are shown on the far right.

behaviour of the distributions (shown in figures 4(*a*)–(*c*)) as the energy E' varies. We note that the energy functional $\varepsilon(s)$ goes as s^2 and s^5, while the volume varies as s^3. Thus $\varepsilon(s)$ dominates for both large and small sizes, while the volume may do so at intermediate ones. (The ratio of the two quantities, equation (50), is minimum at $s = 1$.) Therefore the distribution is broad for large energy inputs and sharpens towards the value $s = 1$ for small E' (see figure 4). At its extreme sharpest, the volume or energy distribution acts as a delta function and the ratio of the energy and volume expectations is given by 3 (equation (40) at $s = 1$), which represents the threshold for energy input per volume a^3. For smaller energy input a maximum-entropy solution does not exist and the distribution is likely to be an irregular, haphazard one.

The general trend of our results, including the interesting sharpening of the distribution at small energy inputs, holds for energy functionals different from that in (40) and (41), provided the energy/volume minimum occurs at finite sizes. This permits the generalization of our results to include a term

$$Cs^z \tag{52}$$

where C is a constant and $z \simeq 4.5$, which represents the energy expenditure in creating internal damage (i.e. cracks that do not join up to form fragments) (Jaeger *et al* 1986a, Aharony *et al* 1986).

The distribution in (49) allows, formally, fragments of size larger than the unit volume, into which the medium was subdivided. To lighten the paradox, one must

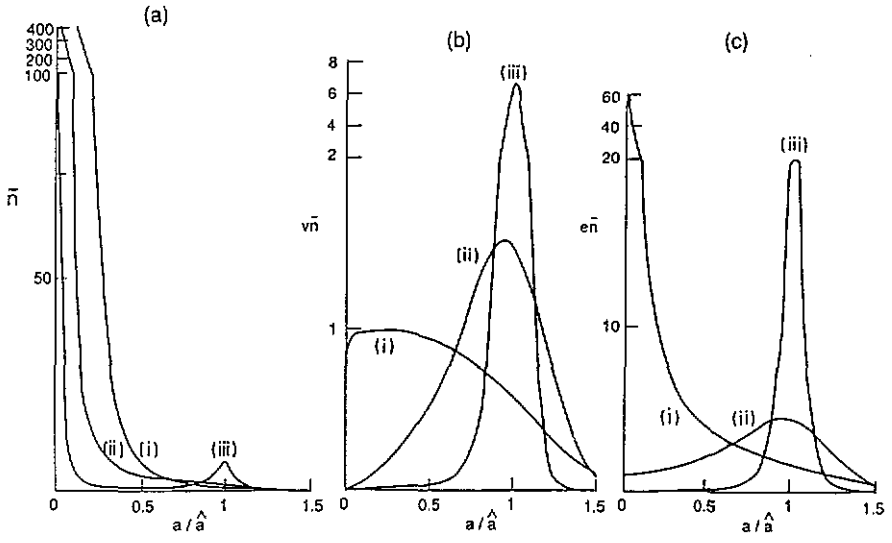

Figure 4. Distributions as a function of the reduced fragment size $a/\hat{a}$ or s; $\hat{a}$ is shown in equation (46). Plotted are: (*a*) $\bar{n}$, the expected number of fragments per unit volume (equation (49)); (*b*) $a^3\bar{n}$, the expected volume (in units of $\hat{a}^3$); and (*c*) $\varepsilon_a\bar{n}$, the expected energy (in units of $2\pi\gamma\hat{a}^2$). In the figures: (i) is for a strong source of fragmentation, $E' = 7.26$, $\beta' = 0.001$, $\nu' = -1.03$; (ii) is for an intermediate strength source, $E' = 3.62$, $\beta' = 1$, $\nu' = 2.48$; (iii) holds for a weak energy input source, $E' = 3.06$, $\beta' = 10$, $\nu' = 29.85$. The distributions sharpen as the energy input decreases. Note the changes in the vertical scales.

regard the distribution as referring to an *ensemble* of fragmenting bodies, in which the occurrence of a fragment larger than a unit adds to the weight of distributions in neigbouring regions.

4. Alternative theories of fragment distributions

Several theories give n_s, the distribution function of fragments of size s (n_s is the number of fragments of size s (s-fragments)). We describe some of these. Summaries from differing viewpoints are due to Dehn (1981), Grady and Kipp (1985) and Campi (1989).

4.1. Geometrical methods

4.1.1. Poisson statistics. The linear, 1D distribution is easily derived and will turn out to be of interest also in higher dimensions (in connection with the so-called Mott distributions). To avoid boundary effects we consider a ring of perimeter length L which is broken up into P pieces by randomly placed cuts (figure 5). The probability of obtaining a piece having a size between s and $s + \mathrm{d}s$, anywhere, is equal to the product of probabilities of placing one cut anywhere (=1), of placing a second cut in the interval $(s, s + \mathrm{d}s)$ measured from the position of the first cut (probability = $\mathrm{d}s/L$), of not having

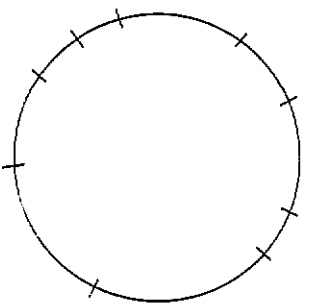

Figure 5. One-dimensional Poisson process. A ring is broken up into n (here 9) segments by n randomly placed cuts.

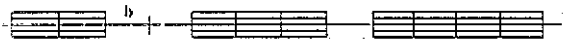

Figure 6. Percolation construction of fragments. Elementary segments of size b are chosen randomly with a probability p, resulting in compound fragments of sizes $2b$, $3b$ and $4b$. An equivalent approach is to choose fragment voids with probability $(1-p)$.

any of the remaining $P-2$ cuts falling in the interval (probability $= [(L-s)/L]^{P-2}$) and multiplied by the number of cuts ($= P-1$) following the first. Altogether

$$\mathrm{d}s\, n_s(P) = 1\,\frac{\mathrm{d}s}{L}\left(\frac{L-s}{L}\right)^{P-1}(P-1). \tag{53}$$

In the limit of L/s and P being large numbers, this reduces to

$$n_s = (1/\bar{s})\exp(-s/\bar{s}) \tag{54}$$

where $\bar{s} = L/P$ is the mean size.

In units where $\bar{s} = 1$ and definition of a new variate z through changes of mean, scale and exponent according to

$$s = [(z - z_0)/\mu]^{1/q}$$

one obtains the Weibull distribution

$$n_z = \frac{1}{\mu q}\left(\frac{z-z_0}{\mu}\right)^{1/q-1}\exp\left[-\left(\frac{z-z_0}{\mu}\right)^{1/q}\right] \tag{55}$$

where $1/q$ is called the shape parameter.

4.1.2. Percolation statistics. In a 1D discrete network consisting of L cells of length b (as shown in figure 6) the 'elementary' segment sizes (cells) are fixed (b). Larger fragments of size sb can form by joining s contiguous fragments, separated from neighbouring ones by the presence of the edges of empty cells whose probability of occurrence on each cell is $(1-p)$. The number of s-fragments is

$$n_s(p) = Lp^{s-1}(1-p)^2. \tag{56}$$

For more details on percolation in one, two, three and higher dimensions, see Stauffer (1979, 1985), Deutscher *et al* (1983) and Zallen (1983).

Table 1. What is fixed and what varies in Poisson and percolation statistics (Campi 1988).

	Poisson	Percolation
Fixed	Number of cuts (P)	Probability of segment (p)
Variable	Probability of segment	Number of fragments

Table 1 sets out the relation between percolation and Poisson statistics. It can be shown (Campi 1988) that the mean or expectation number of fragments of all sizes, namely

$$\sum_{s=1}^{\infty} n_s(p)$$

equals $L(1-p)$ so that in percolation

$$p = 1 - \sum_s n/L = 1 - P/L \tag{57}$$

where we have replaced Σn by P, the number of cuts featuring in the Poisson statistics. Inserting this result in (56) we obtain

$$n_s(p) = \exp[-(P/L)s](L/P)$$

which agrees with the result for Poisson statistics. Size distribution of fragments (or, to use the more common term, of clusters) near the percolation limit $p \rightarrow p_c$ can be shown to be derivable from maximum-entropy principles (section 5). It has also been shown that when the cells are identified with crack positions, fragmentation of a three-dimensional object occurs, within the percolation description, as a sudden transition with a crack concentration $p = p_{cII}$ (Aharony *et al* 1986). This is higher than the usual critical concentration for percolation $p_c(\equiv p_{cI})$. The reason is that at p_{cI} one gets a continuous structure of cracks in the solid without the solid breaking up into pieces. This (namely, fragmentation) occurs only at a higher crack concentration, for $p = p_{cII}$ or higher. Computed fragment statistics are shown in figure 7 and are compared with an experimental distribution (Englman *et al* 1984).

4.1.3. Tessellation. Cutting up a plane with lines or a solid with planes, or, alternatively, forming Voronoi polygons or polyhedra, are further ways of constructing fragments. The essential difference from the physical standpoint is whether one allows lines or planes to cut across each other. (As a rule, true cracks do not intersect except when their propagation velocity is high.) Extensive simulations with random lines in two dimensions by Grady and Kipp (1985) have indicated fragment numbers that decrease exponentially either with the linear dimension ('Mott distribution') or with the area of fragments. In simulations by Sprecher (Jaeger *et al* 1986a, c) the internal structure of fragments was also studied. We mention these, not only to correct the imbalance in this review, which deals almost exclusively with fragment *sizes* whereas other parameters of fragments are also susceptible to statistical treatments, but also to stress the importance of unfinished cracks within the fragment ('internal damage'), which can take up a substantial part of the energy available for fracture.

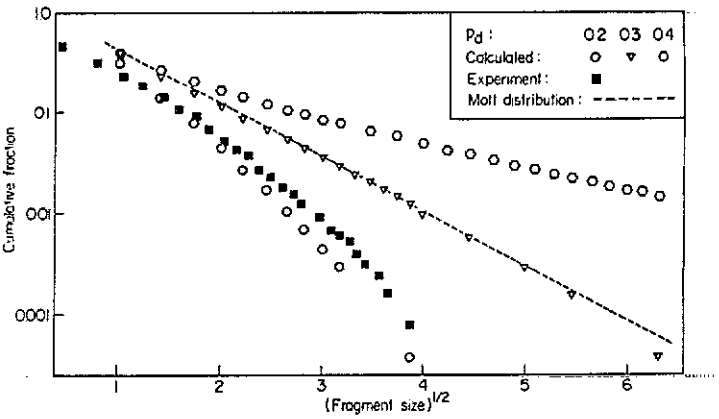

Figure 7. Cumulative fractions (the fraction of two-dimensional fragments being larger than size s) plotted logarithmically against $s^{1/2}$ for intermediate s. Three calculated data sets are shown (open symbols) for the dual lattice percolation probabilities $p_d = 0.2, 0.3, 0.4$ (so that the crack occupation probabilities are $p = 0.8, 0.7, 0.6$) and data points (full squares) for fragments larger than 1 grain, obtained from the explosion of a metal cylindrical shell 0.63 cm thick filled with 47 3DX/31 TNT/22 Al (Sternberg 1973). The line designated 'Mott distribution' represents equation (58).

Leaving aside the question of physical justification for intersecting cracks we can provide a heuristic proof for the Mott distribution generalized to higher dimensions d (>1), namely

$$n_s \propto \exp[-(s/\mu)^{1/d}]. \tag{58}$$

The proof assumes a high density of interesting randomly thrown cracks, such that most fragments have the minimum number of sides, i.e. triangles in a plane and tetrahedra in space. A d-sided object is not yet a fragment, but must await the arrival of another side (the $(d+1)$th crack) to become one. This will fall on the d-sided object at a distance from the opposite apex that follows a Poisson distribution: hence the distribution law in (58), which is Poisson-like in the linear dimension.

4.2. Kinetic distribution

We now describe theories in which a sequence of fragmentation stages is considered, such that each stage retains the memory of the preceding one only by the size of the fragments that are present, not through their state of stress (McGrady and Ziff 1987; Cheng and Redner 1988, Derrida and Flyvbjerg 1987). The results appear to be independent of the physical causes of fracture, yet there is a prediction of 'shattering transitions' in which the numbers of small fragments multiply to infinity as the size of the fragments decreases.

The following integro-differential equation gives the number of fragments $N(s, t)$ of size s at time t in terms of the rate $\nu(s)$ of s-fragments breaking up and the channelling ratio $K(s', s)$ (this quantity gives the fraction of s'-fragments ($s' < s$) created out of the

original s-fragments)

$$\dot{N}(s, t) = -\nu(s)N(s, t) + \int_s^\infty \nu(s')N(s', t)K(s, s')\,\mathrm{d}s'. \tag{59}$$

Constraints include mass conservation

$$\int_0^s s' K(s', s)\,\mathrm{d}s' = s$$

and a postulated mean number $\bar{n}$ of fragments created at each step (e.g. 2 upon cutting) given by

$$\int_0^s K(s', s)\,\mathrm{d}s' = \bar{n}. \tag{60}$$

A problem that can be solved exactly is

$$\nu(s) \propto s^\lambda$$

(e.g. $\lambda = 1$ for random cutting)

$$K(s, s') = b(s/s')/s' \tag{61}$$

(e.g. $b = 2$ for random cutting when $\bar{n} = 2$ in (60)).

The initial condition $N(s, 0) = \delta(s - L)$ for a single piece has the solution

$$N(s, t) = \mathrm{e}^{-st}[\delta(s - L) + 2t + t^2(L - s)].$$

The form in (61)

$$b(s/s') = (s/s')^m$$

gives $\bar{n} = (m + 2)/(m + 1)$. For negative m the number of small fragments rises leading to a 'shattering transition', in which an increasing number of tiny fragments is generated (Ziff and McGrady 1986, McGrady and Ziff 1987).

4.3. Physics-based theories

To my knowledge, apart from the MEM, which forms the subject of this review, there exist no theories of fragment size distribution that are rooted in detailed physical mechanisms. This situation is probably due to the difficulty of disentangling the stochastic and the deterministic aspects of fracture (Grady and Kipp 1989, Jaeger and Englman 1991).

There are indeed physical theories of *fracture*, of which Mott's is perhaps the most notable (Mott 1947, Kipp and Grady 1985, Grady and Kipp 1989). These give, as a rule, mean fragment sizes, but not distributions.

Furthermore there are also models of fracture (mainly in brittle media) and of failure (like yield in ductile solids (Tate 1967, 1969)). Some of these are in the form of extensive computer codes, starting in the early 1970s with the one developed at Stanford (McHugh 1983, Seaman *et al* 1984, Shockey *et al* 1985, Curran *et al* 1987) and simultaneously at Sandia (Davison and Stevens 1972, Davison *et al* 1977), and continuing with several others (Rice 1975, Ravid and Bodner 1983, Ravid *et al* 1987, Kipp *et al* 1980, Taylor *et al* 1985, Kuszmaul 1986, Brandon 1988). However, the quantitative measures

of fracture, failure or damage that are given by the codes, frequently by mapping them onto the interior of the disintegrating body, are not immediately translatable into fragment formation and into a distribution of fragment sizes.

5. Maximum-entropy method and percolation theory

It is of some theoretical interest to establish a link between percolation theory and MEM, though most results are more easily obtained from numerical generation of percolation clusters than by using MEM with the constraints imposed that are in any case the outcome of simulations. In an early effort Kikuchi (1970) used a mean-field treatment to derive critical percolation probabilities by entropy maximization. The agreement with correct values was poor.

The events j in equation (1) for the probabilities p_j are taken to represent the finding of n_s clusters of size s per lattice site

$$p_j \equiv p(n_s, s).$$

We note that in percolation a cluster arises as a connected entity of bonds (or sites) each of which is realized with a fixed probability p. The mean number of s-clusters is

$$\langle n_s \rangle = \sum_{n_s=0}^{\infty} p(n_s, s) n_s.$$

The constraints are, as before,

$$\sum_{n_s} p(n_s, s) = 1$$

for each s and the following relations are given by Stauffer (1981) to define critical indices α, β, γ and δ:

$$\left(\sum_{s=1,\ldots} \langle n_s \rangle \right)_{\text{sing}} \propto \varepsilon^{2-\alpha} \tag{62}$$

$$\left(\sum_{s} s\langle n_s \rangle \right)_{\text{sing}} \propto \varepsilon^{\beta} \tag{63}$$

$$\sum_{s} s^2 \langle n_s \rangle \propto \varepsilon^{-\gamma} \tag{64}$$

$$\sum_{h \to 0,\, s} s(1 - \mathrm{e}^{-hs}) n_s (p \to p_c) \propto h^{1/\delta}. \tag{65}$$

In these relations $\varepsilon \equiv |p - p_c|$, where p_c is the critical occupation probability for percolation, and the subscript 'sing' represents the leading singular part of the sum which remains finite at $p = p_c$.

The MEM solution for the cluster size distribution is

$$p(n_s, s) = L^{-d} \exp(-n_s x_s - \lambda^1)$$

where

$$\begin{aligned} x_s &\equiv_{h \to 0} A + Bs + Cs^2 + Ds(1 - \mathrm{e}^{-hs}) \\ \langle n_s \rangle &= L^{-d} (\mathrm{e}^{x_s} - 1)^{-1} \end{aligned} \tag{66}$$

and λ' is a normalizing constant independent of the size L. The coefficients $A, \ldots, D$

are fitted to satisfy the constraints (62)–(65). The fitting is not easy to carry out since several limiting processes are involved, namely $\varepsilon \to 0$, $h \to 0$, L (size of lattice) $\to \infty$; however, it is clear that for s in some region (s large, yet smaller than L^d) the terms

$$Cs^2 + Ds(1 - e^{-hs})$$

will dominate the expression (66) for x_s. Rewriting this for the given range of s as

$$x_s \simeq C's^2 + D's^3 + O(h) \tag{67}$$

and noting that, for $x_s \ll 1$,

$$\langle n_s \rangle = L^{-d} x_s^{-1} \tag{68}$$

we conclude that the mean number of clusters of size s will show an effective power-law dependence of the form

$$\langle n_s \rangle \propto s^{-\tau} \tag{69}$$

where $2 < \tau < 3$.

For another, heuristic derivation of this result see Zallen (1983). Numerical estimation of cluster numbers near $p = p_c$ gives in three dimensions $\tau = 2.2$, whereas more generally (with $p \neq p_c$) the relationship in (69) becomes modified by a smooth bell-like function of s (Stauffer 1979). However, outsize cluster numbers decrease with size exponentially.

The relation between fragment sizes and percolation clusters appears to have been determined in the first instance by Englman *et al* (1984). A fragment is formed when a piece of material is fully surrounded by linear cracks (in two dimensions) or by crack plaquettes (in three dimensions). The size of fragments is given by the cluster size in the *dual* lattice, defined by placing a bond across a face where a plaquette is missing (or across a line where a crack is missing, in two dimensions) and removing a bond where a crack plaquette is present. The corresponding occupation probabilities in the two lattices are related by

$$p_{\text{dual}} = 1 - p_{\text{crack}}. \tag{70}$$

Fragment distributions for $p_{\text{crack}} > p_c$ (= the critical crack concentration) were obtained by a two-dimensional simulation and followed a modified Mott distribution law, with positive or negative deviations at very large sizes (Englman *et al* 1984) (figure 7).

Let it be remarked that mechanical failure of the solid occurs at $p_{\text{crack}} = p_{\text{cII}}$, so that the condition $p_{\text{crack}} > p_{\text{cII}}$ will be achieved in practice through continued stress loading of the solid, while it is being held together artificially: either by confinement or inertially. In an impact loading (by projectiles, fragments or laser light) the confinement would not be expected to occur and the fragmentation would take place as soon as $p_{\text{crack}} = p_{\text{cII}}$ obtains (Blackman and Goldsmith 1978, MacAulay 1987). Then one would expect to see the relation (69) in effect.

6. Experimental distributions in relation to MEM predictions

6.1. Exploding cylindrical shells

Cylinders made of Armco iron or of heat-treated steel were filled with explosives and

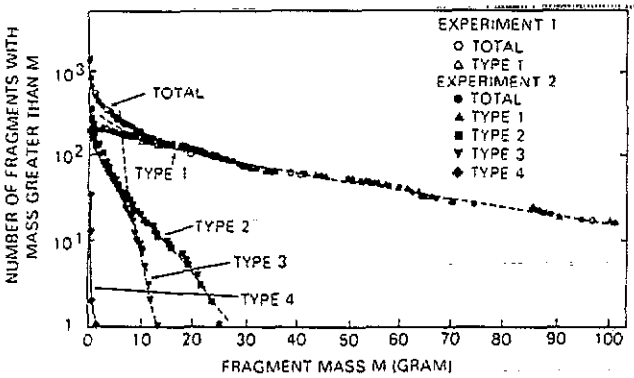

Figure 8. Cumulative fragment distributions from two tests by Mock and Holt (1983) on metal cylinders. Total distributions are shown together with partial distributions for types 1–4, classified according to fragment shapes and origin. The broken curves are theoretical fits in which the contribution of the strain energy term (equation (10)) changes with the type number as follows: $1 \ll 2 \ll 3$. The full curve for type 4 guides the eye.

the resulting fragment size distributions analysed by Mock and Holt (1983) (figure 8). The cylinder walls were about 2 cm thick and the mean diameter about 20 cm, which makes it questionable whether to apply two-dimensional (shell-like) or three-dimensional modelling. However, the authors separated the fragments in accordance with a characterization scheme based on the nature (brittle or shear) of the fracture surfaces. Different fragment types (labelled type 1–4 in figure 8) had different mean mass per fragment. The type with the largest mean mass (type 1 in figure 8) followed a roughly exponential cumulative distribution, except for small sizes, as a function of the fragment mass M. However, the types with smaller mean masses (types 2–4) showed a decrease with mass that was faster than that. The explanation is straightforward in terms of the formulae (10), (18) and (19). The small mean mass is indicative, by (26), of larger strain rate $\dot{\varepsilon}$. In formula (10) for the exponent in the distribution $\langle n_a \rangle$, equation (19), the strain-rate term goes as a^5, or the 5/3 power of mass, to be compared with the inertial term going as the mass, which is expected to be dominant for the smaller strain-rate, type 1, fragments.

A large number of fragment distributions arising from explosively shattered cylindrical shells were obtained by Sternberg (1973) with variations in the shell composition and treatment and in the explosive. A simple exponential (Mott-type) distribution failed to account for the data over the whole mass range and consequently a distribution was synthesized from three separate exponentials, appropriate to small, medium and large sizes. The MEM distribution in two dimensions is given as a function of linear dimension a by equation (19), where x_a takes the form analogous to equations (10) and (18)

$$x_a \propto Aa + Ba^2 + Ca^3. \tag{71}$$

With suitable choice of the parameters A, B and C the MEM fits quite well the results of Sternberg (1973) for two combinations of steel and explosive (figures 9(*a*) and (*b*)).

Exploding mild-steel tubes with wall thickness/diameter ratios ranging from 0.05 to 0.17 were investigated by Stronge *et al* (1989), regarding the dependence of the fragment size distribution on the fracturing mechanism. This was varied through changing the explosive (charge) mass/metal mass (C/M) ratio over a 10-fold range. A two-dimen-

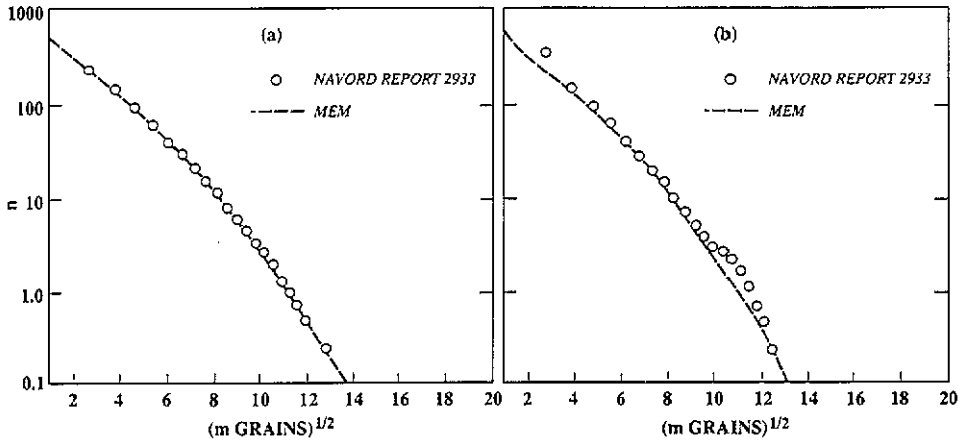

Figure 9. Distributions of fragments from an exploding metal shell versus the square root of the fragment mass (Sternberg 1973). The broken curves show two-dimensional MEM distributions, equation (71), in which a^2 represents the fragment mass and the parameters take the following values (in mass units of milligrains): (*a*) $A = 0.22$, $B = 0.05$, $C = 0.05$; (*b*) $A = 0.22$, $B = 0.05$, $C = 0.0625$.

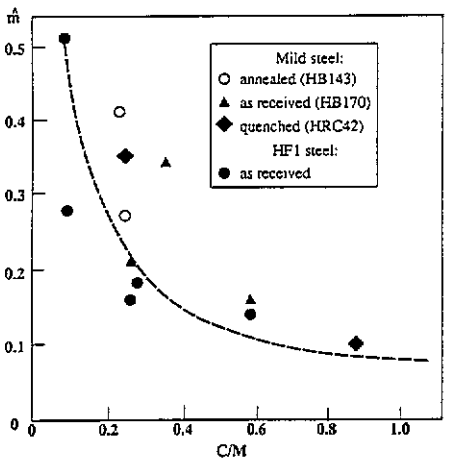

Figure 10. Mean mass $\hat{m}$ of mild-steel fragments versus the charge/metal mass C/M ratio (Stronge *et al* 1989). The broken curve shows the theoretical result of equation (73).

sional Mott distribution was assumed without obvious evidence. The mean mass decreased with C/M as seen in figure 10.

In the theory the most likely mass $\hat{m}$ ($\propto a^3$) varies with the strain rate as

$$\hat{m} \propto \dot{\varepsilon}^{-2}. \tag{72}$$

We can relate the explosive/metal mass ratio to the strain rate by using the Gurney relation (Jones *et al* 1980):

$$v_0 = [2G/(0.5 + M/C)]^{1/2} \tag{73}$$

where v_0 is the velocity with which the outer part of the cylinder moves and G is the

energy release by the explosive per unit mass. We associate the strain rate with v_0/inner cylinder radius and obtain from (72) and the expression for v_0

$$\dot{m} \propto 0.5 + (M/C). \tag{74}$$

The broken curve in figure 10 indicates quite reasonable agreement with the experimental data points.

On the basis of a large number of fragmentation experiments with exploding cylinders, Lin *et al* (1989) proposed a numerical fit for the number of fragments N_{tot} as a function of the dimension, hardness and composition of the cylinder and of C/M, the charge/metal mass ratio:

$$N_{tot} = 177t + 107CP - 0.39H + (C/M)(-3250 + 10462CP - 2.52H) + 34.5$$

where t is the thickness of the cylinder (cm), H its (Vickers) hardness and CP the carbon content percentage. (It is appropriate to remark here that Mott's involvement in the mechanism of fracture arose during the Second World War from his investigation into the difference between N_{tot} in Allied and German shells. Eventually it was all traced to CP, which increased the metal brittleness) (Mott 1984, private communication).)

6.2. Fragments in mining operations

It might be thought that a distribution with three free parameters, such as given by equations (10) and (19), is bound to agree with practically any experimental curve, especially when the cumulative distribution is plotted (on a logarithmic scale). The following example shows that this is not the case and that when sufficiently accurate data are plotted for a wide enough fragment size range the MEM distribution postulated in equation (10) can be discredited and, instead, another MEM distribution with different constraints appears to operate. Unfortunately, the latter constraints do not have any simple physical meaning.

Boreholes of 3.2 cm diameter were filled with Donarite and exploded in an underground site of the Rotem (Negev, Israel) oil-shale fields of the PaMA company (Jaeger *et al* 1986b). Post-explosion fragments were kept in place by chicken wire, collected from several locations and layers around the original boreholes, the pieces individually weighed and their distributions determined for each location. The derived distributions differed significantly, according to the distance of the locations from the centre and somewhat on their orientations (the terrain was anisotropic due to major faults). However, (quite remarkably) all distributions could be brought into coincidence by scaling the sizes at each location with a scale factor $\lambda(R)$ that increased monotonically with the distance R of the location from the borehole as $R^{1.75\pm0.3}$ (figure 11).

We have not found it possible to fit the collapsed distribution with any set of Lagrangian parameters appearing in equation (19). A least-squares fit of the parameters was not done, but the intuitively 'best' fits shown in the figure as broken curves are evidently inadequate to reproduce the results over the four decades of linear size variation. A MEM distribution of the form

$$n_a = \{\exp[(a/a_1) + b\log(a/a_0)] - 1\}^{-1} \tag{75}$$

was found to fit the observed cumulative weight distribution

$$\int_{a_0}^{a} \rho \dot{a}^3 n_a \, da$$

reasonably well, with the choice and interpretation of the parameters as follows:

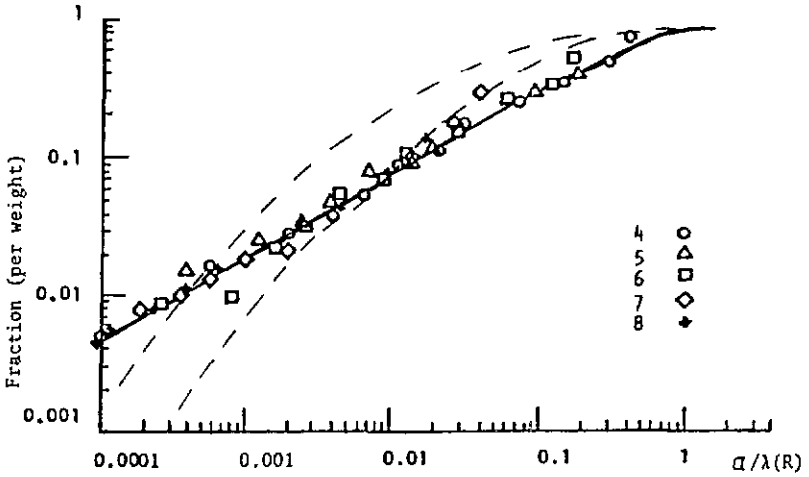

Figure 11. Cumulative weights of mined oil shale against normalized linear fragment size (Jaeger *et al* 1986b). Results from five regions, numbered according to increasing distance from the borehole, lie on the same curve when a length scale parameter $\lambda(R)$ is adjusted. The broken curves are based on equations (18) and (19), and are plainly inadequate. The full curve is obtained using equation (75) with parameters given in the text.

a_1 (upper cut-off of size) $= 2\lambda(R)$

a_0 (lower cut-off of size) $= 8 \times 10^{-5}\lambda(R)$

b (effective inverse power of distribution) $= 3.43$.

The two functions in n_a (a and $\log a$) indicate the existence of physical constraints (appendix 1) on the distribution. The constraint on a can be accorded some physical meaning in terms of dense cracks (along the lines of the discussion in section 4.1.3); however, the constraint related to $\log a$ is obscure.

In a similar type of experiment, though on a much smaller scale, Curran *et al* (1977) collected the ejecta from the crater formed by high explosives in contact with the surface of fine-grained quartzite rock. The number of fragments per unit fragment radius a, n_a, follows (for about five decades of variation in n_a) remarkably well the power-law relationship

$$n_a \propto a^{-2.1} \tag{76}$$

indicating the importance of the surface energy term (proportional to a^2) in equation (1). (Figure 4.10 in Curran *et al* (1987) shows the cumulative number of fragments. The theoretical fit in the figure suffers from identification of fragment and crack size distributions in their equation (4.6).) The surface term is indeed expected to dominate for small fragments ($a \ll \hat{a}$) and for such fragments we anticipate a power-law behaviour, like that in (76).

6.3. Distribution of space debris

Man-made debris in space exceeds the number of natural meteoroids and represents a danger to spacecraft (Kessler 1985, Rajendran and Elfer 1989). The fragments arise from defunct space vehicles that have broken up, exploded or become involved in collisions. Added to this are solid fuel particles. Three distributions are given as a function of the mass m (Johnson and McKnight 1987) or of the size s.

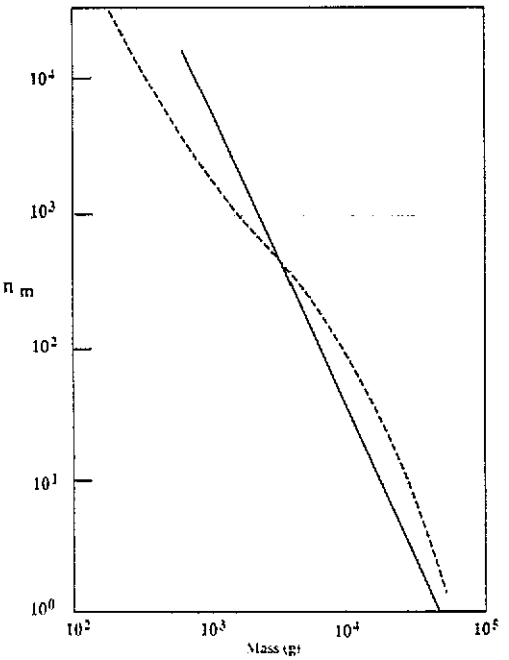

Figure 12. Distribution of masses in space due to defunct, broken-up satellites. Broken curve: observation (described in the text). Full curve: fit by a power law based on percolation theory.

Small fragments due to collisions have a power-law (fractal-like) distribution.

$$n_s = C_1 s^{-1.75}. \tag{77}$$

Larger fragments, but not exceeding 1960 g, follow the distribution

$$n_s = C_2 m^{-1/2} \exp(-0.0575 m^{1/2}) \tag{78}$$

with m in grams. For even larger fragments, caused mainly by explosions, one finds

$$n_s = C_3 m^{-1/2} \exp(-0.0205 m^{1/2}). \tag{79}$$

The coefficients C_1, C_2 and C_3 depend on the total masses included in the distribution and are not relevant to the expected distribution from a single event. In figure 12 we have combined the three distributions in one smooth curve and compared the resultant with the percolation result $n_s \propto s^{-2.2}$.

The experimental distribution drops slower than this prediction for small sizes and faster for larger fragments. In some sense, the prediction represents a simple averaging over the full range.

6.4. Charged atomic clusters

Clusters consisting of 10–10^2 atoms or molecules are of interest theoretically (as transition species between molecules and solids) and experimentally (e.g. as potential catalysts). A review of early results was given by Phillips (1986). Clusters can be formed from the gaseous phase by accretion or condensation after passing through a jet (Levinger *et al* 1988, Rayane *et al* 1989) or from an impacted solid by sputtering (Weiland *et al* 1989). The distribution of cluster masses can be obtained by time-of-flight mass spectrometry and depends on the conditions under which clusters form (e.g. the ambient

gas pressure). The distributions are frequently peaked (as in rare-gas clusters Ar_m^+) at magic numbers associated with favourable conditions for packing or with bunching of electronic (binding) energies (Knight *et al* 1984, Stephens and King 1981). The broad envelopes of mass distribution, which are our concern here, generally possess a maximum, though exceptions from this situation do exist. Thus, counts of positively charged uranyl acetate clusters decrease monotonically for cluster sizes of up to 50 units, while the negatively charged clusters show a maximum. Charged clusters are easier to observe in experiments than neutral ones.

Writing the MEM distribution as a function of the mass m in the form appearing in equation (19), namely

$$n_m = (e^{x(m)} - 1)^{-1} \tag{80}$$

where

$$x(m) = \sum_r a_r m^r \tag{81}$$

(cf equation (19)), we note that, for n_m to have a maximum at a non-zero mass, at least some of the exponents in the above sum must be negative. We recall that the energy equipartition constraint of Griffith (1943) described in section 3.1 led to a negative exponent $r = -1/3$.

This arose from supposing that the available energy was first distributed equally between all atoms or molecules, so that each atom absorbs a part of the order m^{-1} and then expends this on the surface energy (which is proportional to $m^{2/3}$). In addition, one can suppose that the absorbed energy is also expended on creating a transverse dynamic tension (analogous to the strain energy term in (10)) proportional to $m^{5/3}$. Then in the sum (81) one also has a term with exponent $r = 2/3$.

A fitting of expressions (80) and (81) to the mass distribution data of Levinger *et al* (1988) for Ar_m^+ was made, with the choice of the coefficients in (81), given (in Ar mass units) by

$$a_{-1/3} = 8.5 \qquad a_{2/3} = 15$$

(figure 13). Fits of similar goodness were achieved to other data obtained by the above authors for Ar_m^+ and by Rayane *et al* (1989) for positively charged indium and lead clusters, by choice of slightly different coefficients. The formation of small ions ($m < 5$) is probably due to factors not included in the energy constraint and for these the misfit is excusable. It is notable that the skewness of the experimental distribution is reproduced by the theory. To end this section, we wish to stress this adaptation of the MEM to fragment formation by growth, rather than by disintegration, as in the rest of this article.

6.5. Droplets

The distribution of droplets in a spray is important for the operation of fuel injection engines, for painting and elsewhere. The liquid column or sheet is unstable due to fluctuations and breaks into droplets that are subject to several forces (inertial, nozzle pressure, aerodynamic drag by the ambient gas). Studies have been made of droplet sizes and velocities as a function of pressure and distance along the flow and perpendicular to it. Experimental investigations use phase/Doppler techniques (Bachalo *et al* 1988, Sellens 1989). For a description of the subject, including an introduction to size distribution results, the book of Lefebvre (1989) is of use. MEM were applied to obtain the

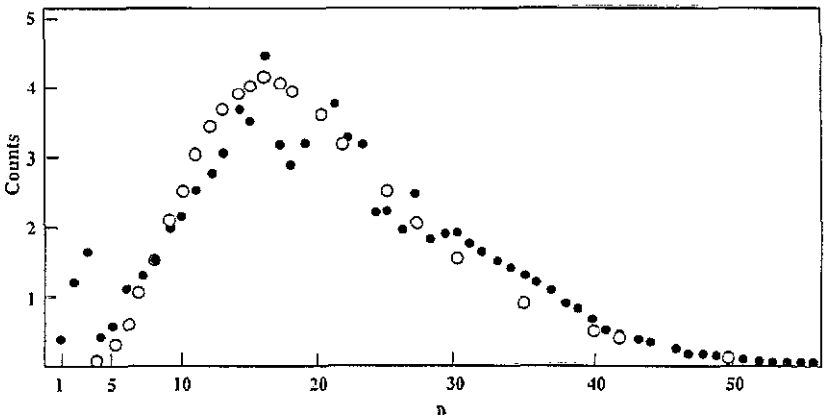

Figure 13. Counts of charged argon clusters against argon mass number n. Full circles: experimental data obtained by time of flight (Levinger *et al* 1988). Open circles: theoretical results (equations (80) and (81) with parameters shown in text).

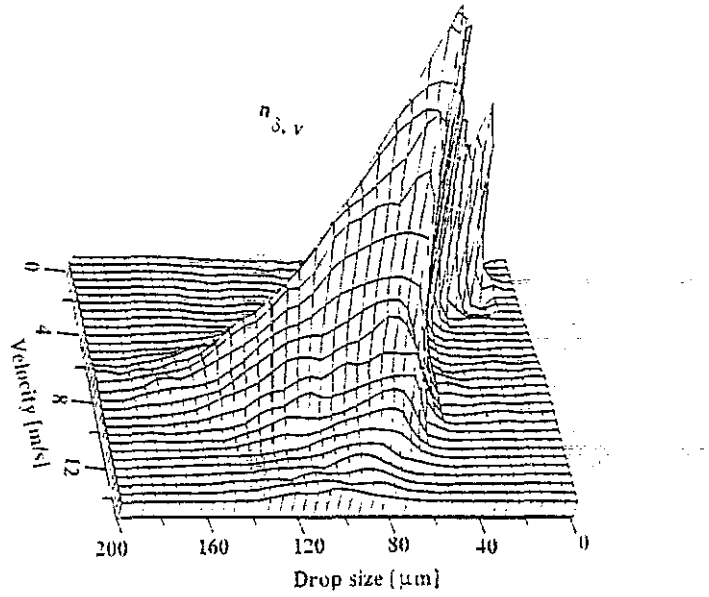

Figure 14. A typical surface of droplet distributions as a function of linear size and downstream velocity. (After Sellens (1989).)

joint, velocity size distribution function, employing constraints on the total mass, the surface energy, kinetic energy and total momentum (Sellens and Brzustowski 1986, Sellens 1989). It is, however, stated that 'it is simpler to measure the resulting spray, rather than the input conditions' (Sellens 1989). An example of the experimentally determined joint distribution is shown in figure 14 as a function of the droplet size δ (typically $10^2\,\mu$m) and velocity v. The theoretical distribution has the form shown in equation (A1.3), where ϕ are functions of δ and v entering the constraint expressions.

The marginal size distribution reproduces the observations satisfactorily, but in the v–δ correlations there are discrepancies. The use of correlations in MEM has been described (Englman *et al* 1988b). In the experiments the mean velocity decreases with droplet size, due to the aerodynamic drag being more effective for small droplets, while the prediction shows constancy (since the drag is not formulated as a constraint). This situation differs from that typical for fragmentation of solids, where smaller-sized fragments fly off faster than larger ones (Grady *et al* 1985). The latter result can in fact be regarded as a direct consequence of the momentum and kinetic energy constraints, which introduce the functions

$$\phi = v\delta^3 \qquad \text{and} \qquad v^2\delta^3$$

in the exponential in (A1.3), so that (the Lagrange multiplier λ' being presumed positive) smaller sizes lead to higher speeds.

In a related subject, although many orders of sizes away, the condensation of interstellar clouds by fluctuations was considered (Kiguchi *et al* 1988, Narita *et al* 1988, Stahler 1983). Blobs, stars of 10^{-3}–10^{-1} solar masses, materialize by collapse and fragmentation, and so do rings of up to 10^2 solar masses from rotating clouds.

Returning to Earth, we note the exponential distributions with a low size cut-off in one-dimensional composite fibres (Wagner and Eitan 1990).

6.6. Nuclear disintegration

A percolational critical point has been shown to operate in nuclear disintegration (Campi 1988, Gross 1990). High-velocity gold ions impinging on emulsion produced a distribution of fragments with charges between 1 and 79 (= the number of charges on Au), observed by Waddington and Freier (1985). Campi (1988) has found correlations between the second, first and zeroth moments of the size distribution that strongly resembled the correlations in a percolative system near $p = p_c$. (Use was made of the relation (57) originally noted by him.)

The largest fragment in disintegration can be associated with the cluster that tends to percolate (i.e. extend throughout the media) at critical concentration p_c and whose mass density is known as the fractal dimension (Zallen 1983). In a finite-sized nucleus the largest fragment size is related to the total mass of the nucleus by finite size scaling (Stauffer 1979). By proper identification of the largest fragments and of p_c in the experimental data of several atoms, Campi (1989) has found a fractal dimension that agrees with that for the percolating cluster. In the same paper Campi proposed a valuable hypothesis, elaborated by Gross (1990), for the ergodicity of the percolation model, which is also pertinent to the ergodic behaviour underlying the use of MEM. According to this, the sudden fracturing event leaves the incipient fragments in an excited state, which probes all distributions in an ergodic fashion. At a later stage, a relaxation occurs in which mass distributions do not change any more.

7. Conclusions

Fragment distributions based on maximum entropy not only have theoretical soundness (alas, not universally acknowledged), but they also possess the merits of containing both probabilistic and physical components and of accommodating naturally exponential and inverse power behaviours (as a function of particle size). Various experimental

distributions have been well reproduced by MEM, though other *ad hoc* laws can do this too, except in the extremities of very small and large fragments. Some characteristics of empirical distributions (like fractal nature or possession of a hump) have their signature in MEM, leading (with some measure of certainty) to physically significant conclusions as to the breaking mechanism.

Concerning useful extensions of the subject, one envisages future uses of maximum entropy for non-equilibrium phenomena, like rates of catalytic reactions involving particulates or fluid flow in fragmented media.

Acknowledgments

I gladly affirm the strong supporting role of Zeev Jaeger in the preparation of this article and the value of advice received from Rafi D Levine. This work was supported in part by the US Air Force Office of Scientific Research, Air Force Systems Command, USAF, under Grant No. 83-0374. The US Government is authorized to reproduce and distribute reprints for Governmental purposes notwithstanding any copyright notation therein.

Appendix 1. On maximum entropy

A1.1. Basics

In the basic formulation of the maximum-entropy method (MEM) one maximizes the information entropy S with respect to the probabilities p_j of events j, subject to the R observational inputs or constraints written as:

$$\langle \phi^r \rangle = \sum_j p_j \phi^r(j) = \int p(j)\phi^r(j)\,\mathrm{d}_j \qquad r = 1, 2, \ldots, R. \tag{A1.1}$$

Summation or integration (for continuous variates) is over the range of variation.

Formally, and in practice, one maximizes the following function of probabilities, named Lagrangian (Rivier *et al* 1989):

$$L(\{p\}) = -\sum_j p_j \log p_j - \lambda^1\left(\sum_j p_j \phi^1(j) - \langle \phi^1 \rangle\right) - \ldots - \lambda^R\left(\sum_j p_j \phi^R(j) - \langle \phi^R \rangle\right) \tag{A1.2}$$

obtaining for the MEM probabilities

$$p_j = \exp[-\lambda^1 \phi^1(j) - \ldots - \lambda^R \phi^R(j)] \tag{A1.3}$$

in which the Lagrange multipliers are fitted to satisfy the constraints (A1.1). As already noted in the introduction, the MEM solution is characterized by a smooth behaviour as a function of j.

Examples of constraints are first, the normalization condition on the probabilities,

$$1 = \sum_j p_j = \int p(j)\,\mathrm{d}j \tag{A1.4}$$

and observed averages like

$$\langle j \rangle = \sum_j p_j j \qquad \text{and} \qquad \langle j^2 \rangle = \sum_j p_j j^2$$

etc. Acceptable constraints are also observed frequencies of events, in the form

$$\langle \delta_{jj_0} \rangle = \sum_j p_j \delta_{jj_0}. \tag{A1.5}$$

Because of the presence of the singular function δ_{jj_0} or $\delta(j - j_0)$ in the exponent of p_j in (A1.3), the MEM solution is in general no longer smooth, but is probably still more conservative than alternative non-MEM solutions.

In fact, the range of the variate j can also be written as a constraint, in the sense of zero frequency of occurrence outside the range.

A1.2. Priors $\Pi(j)$

These are introduced as generalizations of the summations over the events in (A1.2), with the purpose of weighting each event by a factor $\Pi(j)$, so that the entropy becomes

$$S_\Pi = -\sum_j \Pi(j) p_j \log p_j \tag{A1.6}$$

and a typical constraint

$$\langle \phi \rangle_\Pi = \sum \Pi(j) p_j \phi(j). \tag{A1.7}$$

The priors are weights ascribed *a priori* (that is, without regard to observations) to each event and correspond to 'measure' in set theory. Skilling (1989) writes about them thus: 'Π is the Lebesgue measure associated with [the variable], which must be given before an integral can be defined.' A possible probabilistic interpretation identifies the priors with subjective beliefs or reliance attached to the events. Physically, priors may be related to instrumental effects. An example of this is the photofragmentation studies of Ar_n^+ cluster ions (section 6.4). In making a statistic of the number of detached ions as a result of photoabsorption, the data must be weighted by the dependence of the photoabsorption cross section on the size (n) of the cluster ion (Levinger *et al* 1988).

If the priors are known or postulated there is no difficulty since one can proceed as follows. Let the weighted probabilities of events be denoted by

$$P_j = \Pi(j) p_j. \tag{A1.8}$$

Then we rewrite (A1.6) and (A1.7) as

$$S_\Pi = -\sum_j P_j \log P_j/\Pi(j) \qquad \text{and} \qquad \langle \phi \rangle_\Pi = \sum P_j \phi(j). \tag{A1.9}$$

We maximize the Lagrangian with respect to P_j. Equation (A1.8) is the solution, with p_j given in (A1.3). The functional form of the exponential part, i.e. the dependence

on $\phi^1, \phi^2, \ldots, \phi^R$, is not affected by the introduction of the prior, but the pre-exponential part is, and so are the numerical values of the Lagrangian multipliers, λ^1 to λ^R. This follows since these are given by the implicit equations

$$\langle \phi^r \rangle = \sum_j \phi^r(j)\Pi(j) \exp[-\lambda^1 \phi^1(j) - \ldots - \lambda^R \phi^R(j)] \tag{A1.10}$$

which contain Π. In the use of MEM as a pure predictive tool for natural phenomena, the dependence of the solution on the priors raises the question: 'Which is the best prior?' (Jeffreys 1961, Jaynes 1983, Englman *et al* 1988a). It seems that no satisfactory answer exists at this stage, except perhaps to say that the MEM solution is unique as far as its asymptotic exponential dependence is concerned but not regarding the prefactor.

The following, related problem appears to have been solved (Rivier *et al* 1989). Suppose that there exist a number K of possible priors (e.g. K alternative beliefs or hypotheses), given by

$$\Pi^k(i) \qquad k = 1, \ldots, K. \tag{A1.11}$$

What linear combination

$$\Pi(j) = \sum_{k=1}^{K} p^k \Pi^k(j) \tag{A1.12}$$

gives the best prior? 'Best' is to be considered in terms of incoming information, since before that information we suppose (democratically) that all priors have the same weight. The proposed solution relies on maximizing the following generalized functional of the event probabilities and of the weights p^k:

$$\mathcal{L}(\{P_j\}, \{p^k\}) = -\sum_j p_j \log P_j/\Pi(j) - \sum_r \lambda^r \Big(\sum_j P_j \phi^r(j) - \langle \phi^r \rangle \Big) - \nu \sum_{k=1}^{K} p^k \log p^k \tag{A1.13}$$

where Π is defined in (A1.12) and ν quantifies the credit accorded to the diversity of views relative to factual evidence. (Rivier *et al* (1989) assumed $\nu = 1$, which is as good a starting point as any.) The MEM weights are

$$p^k = \exp(X_k/\nu) \Big/ \sum_k \exp(X_k/\nu) \tag{A1.14}$$

where

$$X_k = \sum_j \Pi^k(j) \exp\Big(- \sum_r \lambda^r \phi^r(j) \Big) \tag{A1.15}$$

is the overlap between the prior Π^k and the exponential part of the MEM probability. The dependence of the weights p^k on the incoming evidence is through the expectation values $\langle \phi^r \rangle$ and the resulting values of λ^r.

It is interesting to compare this result with the Bayesian rule (Jaynes 1985, Jeffreys 1961, Skilling 1989)

$$P(k|\langle \phi \rangle) = P(k)P(\langle \phi \rangle | k)/P(\langle \phi \rangle) \tag{A1.16}$$

whose meaning in the present context is the following. The probability $P(k|\langle \phi \rangle)$ for the hypothesis (or prior) k, given that the mean has the observed value $\langle \phi \rangle$, is equal to the probability $P(k)$ of the same hypothesis, irrespective of the observation on $\langle \phi \rangle$,

multiplied by the probability $P(\langle\phi\rangle|k)$ of obtaining $\langle\phi\rangle$ on the basis of the k hypothesis and divided by the probability $P(\langle\phi\rangle)$ of obtaining the observation $\langle\phi\rangle$ on the mean. The Bayesian interpretation of the result in (A1.14) and (A1.15) is then, in an obvious notation,

$$P(\langle\phi\rangle|k) = \exp[X_k(\langle\phi\rangle)/\nu] \Big/ \sum_{\langle\phi\rangle} \exp[X_k(\langle\phi\rangle)/\nu] \tag{A1.17}$$

$$P(\langle\phi\rangle) = \sum_k P(\langle\phi\rangle)|k) \tag{A1.18}$$

$$P(k) = \sum_{\langle\phi\rangle} \exp[X_k(\langle\phi\rangle)/\nu] \Big/ \sum_k \sum_{\langle\phi\rangle} \exp[X_k(\langle\phi\rangle)/\nu]. \tag{A1.19}$$

We now recognize the merit of MEM as providing a systematic method for differentiation between alternative hypotheses (beliefs, physical mechanisms) on the basis of incoming evidence. The shortcoming of MEM is that much of our knowledge, understanding and 'feeling' for the behaviour of the physical system that is not phrased explicitly in the form of constraints receives no expression in the predictions.

Appendix 2. Fracture diversity

A2.1. Causes of fracture

Mechanical fracture is frequently the physical process that precedes and causes fragmentation, though such is not the case in droplet formation (section 6.5), photofragmentation, nuclear events (section 6.6), desorption, etc.

At the root of the fracture of solids is the breakage of atomic or molecular bonds. Simulations of the fracture process on this fundamental level have been numerous (Esterling 1979, Latanision and Pickens 1983, Paskin *et al* 1983, Thomson 1986, Thomson and Fuller 1982). There are three considerations that render this approach of limited scope or excessive difficulty. ('Clearly, for the near term, there is not likely to be a first-principles calculation of a crack tip' (Thomson 1986).)

(i) Subsequent to fracture there is a large-scale relaxation, i.e. shift of particle positions, in the solid surrounding the created discontinuity (or bond breakage) (Mai and Lawn 1987). Thus a presumed single-particle scission is in truth a many-particle effect. Owing to this and other causes, nominal atomic surface energy densities (the energy input needed to cut atomic bonds over a unit surface) exceed observed surface energy densities (the quantity that enters Griffith's expression for the fracture strength (Griffith 1920)) by two or three orders of magnitudes (Sih 1983).

(ii) The region in the vicinity of the crack tip shows (even in brittle solids) plastic behaviour. Such behaviour is difficult to model with elastic strings (obeying Hooke's law, at least up to a range, as is frequent practice in atomistic simulations) or to formulate fracture in the context of ordinary thermodynamics.

(iii) The applied stress that brings about breakage does so not by initiating and opening up a single void, but by giving birth to a number of microcracks (or microvoids, in ductile materials), which then interact and ultimately merge to propagate the macrocrack (Curran *et al* 1987). This viewpoint is becoming increasingly more firmly established as better observational techniques on the microevent length scale ($<1\ \mu$m) and fast timescales ($<10^{-9}$ s) are available (Bowling *et al* 1987, Faber *et al* 1988). In

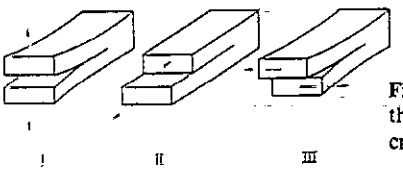

Figure 15. The three modes of fracture, showing the direction of the stresses with reference to the crack about to be opened.

fast processes (which cause most of the fragmentations treated in this review) the proliferation of microcracks is particularly decisive. This can be understood by the following argument.

Two events taking place in the solid at a separation of Δl develop independently of each other, provided the ratio propagation velocity/Δl is smaller than the relative strain rate $\dot{\varepsilon}/\varepsilon$ due to an externally applied force. With propagation or sound velocities of the order of 10^3 m s^{-1}, strains $\varepsilon \sim 10^{-1}$ and strain rates $\dot{\varepsilon} > 10^6$ s^{-1} (appropriate to explosive breakage), two cracks at distances larger than

$$\Delta l = 10^{-4} \text{ m} \tag{A2.1}$$

prefer to develop independently, rather than let stress release operate by the growth of one crack (presumably the larger one). Likely, the true distances are smaller than that in (A2.1).

A2.2. Fracture in real-life situations

Modalities of fracture in real-life situations are so multifarious that either an all-embracing treatment or one that is based on a single viewpoint is likely to court failure. Therefore, in the following brief essay we emphasize just the different varieties of modes and forms that fracture can take, as seen by several leading workers in the field. The putative moral from this exercise is that in view of the wide spectra of manifestations one is inevitably thrown back to a stochastic description, like that provided by MEM.

The three modes of external stress with respect to the fracture plane, shown in figure 15 and traditionally known as modes I, II and III, are perhaps the least relevant subdivision of fracture-causing processes, since in most of the fragmentation situations discussed in this review the imposed stress appears in mixed modes. This claim is supported by recent observation of crack types in indented ceramics where also the variety of observed cracking sequences has defied systematization in terms of the nature of the applied load (Cook and Pharr 1990). In talking about the initiation of microdefects, one should perhaps temper the claim for an excessive variety in the following sense. Theories of microvoid nucleation, pioneered by Raj and Ashby (1975) in the context of polycrystalline metals, apparently lead to the same, exponential microflaw size distribution (as a function of the linear flaw dimension), no matter what are the details of the flaw-producing mechanism (Curran *et al* 1987).

An important differentiation is between ductile and brittle fracture, the former being characteristic of most metals, metallic alloys and also of high temperatures and low strain rates, whereas the latter operates in rocks, ceramics, etc, at low temperatures and in fast processes (ubiquitously). Typical flaws are, respectively, voids and cracks. A seminal contribution to fracture processes in a metal ring was made by Mott (1947), who used momentum conservation to calculate the time that stress unloading requires to propagate away from the point of fracture until completion of

failure. For elaboration of this theory we refer to Kipp and Grady (1985). For brittle fracture the corresponding advances are due to Griffith (1920) and Irwin (1957), who formulated an energy-balance-based criterion for the run-away motion of cracks. This will happen when the release of stress energy around a growing crack (regarded as a free surface) exceeds the energy expenditure involved in the crack extension.

Using considerations similar to those given in the previous section regarding the rate dependence of defect activation, Grady and Kipp (1989) distinguished between fracture processes that are dominated by the input stress energy and those by the defect population density. In the former the rate of fracturing depends on the loading intensity; in the latter strengthening the load does not enhance fracture, since the number of microdefects is insufficient to respond to the added load and the energy gets diverted into other channels (like mass motion or heat). As a rule, high strain rates ($\dot{\varepsilon}$) ensure the creation of sufficiently dense defect population so that fracturing rate becomes energy-dominated, while low $\dot{\varepsilon}$ creates defect bottlenecks.

Experimentally observed crack-tip shapes fall into three broad categories that link the fracture process both to the brittle–ductile material characterization and to the emission of dislocations from and around the growing crack (Thomson 1986). Sharp knife-edged cracks cleave, have brittle characteristics and displace, but do not generate, dislocations as they advance; wedge-shaped cracks emit new distinctly oriented dislocations that advance to a free surface as the crack grows; finally, blunt or rounded crack tips emit a mixture of dislocations, typical of plastic behaviour. The implication of dislocations in crack motion is well recognized (it is akin to the molecular basis of gas thermodynamics), and the dislocation-based approach has had its successes in relating metal hardness to granularity (Hirth 1972). However, difficulties of treatment have so far prevented a broadly significant contribution to crack growth and fracture. Perhaps recent advances in lattice gauge theories might point to new directions, though at this stage this clearly seems a remote subject on which to pin our expectations (Kleinert 1989).

References

Aharony A, Levi A, Englman R and Jaeger Z 1986 *Ann. Isr. Phys. Soc.* **8** 112

Bachalo W D, Rudoff R C and Brena de la Rosa A 1988 *AIAA 26th Aerospace Sciences Meeting (Reno, NA)*

Bianchi R, Capaccioni F, Cerroni P, Coradini M, Flamini E, Martelli G and Smith P N 1984 *Astron. Astrophys.* **139** 1

Blackman M E and Goldsmith W 1978 *Int. J. Eng. Sci.* **16** 1–99

Blink J A and Hoover W G 1985 *Phys. Rev.* A **32** 1027

Bowling G D, Faber K T and Hoagland R G 1987 *J. Am. Ceram. Soc.* **70** 849

Brandon D G 1988 *Materials at High Strain Rates* ed T Z Blazynski (London: Elsevier) pp 187–217

Campi X 1988 *Phys. Lett.* **208** 351

—— 1989 *J. Physique Coll.* **50** CR-183

Capaccioni F, Cerroni P, Coradini M, di Martino M, Farinella P, Flamini B, Martelli G, Paolicchi P, Smith P N, Woodward A and Zappola V 1986 *Icarus* **66** 4871

Cheng Z and Redner S 1988 *Phys. Rev. Lett.* **60** 2450

Cook R F and Pharr G M 1990 *J. Am. Ceram. Soc.* **73** 787

Curran D R, Seaman L and Shockey D A 1987 *Phys. Rep.* **147** 1

Curran D R, Shockey D A, Seaman L and Austin M 1977 *Proc. Symp. on Planetary Cratering Mechanics—Impact and Explosion Cratering* ed D I Roddy, R O Pepin and R B Merrill (Oxford: Pergamon) p 1057

Davison L and Stevens A L 1972 *J. Appl. Phys.* **44** 668

Davison L, Stevens A L and Kipp M E 1977 *J. Mech. Phys. Solids* **25** 11
Dehn J 1981 *Aberdeen Proving Ground, Maryland, Report No.* ARBBL-TR-02332
Denbigh G and Denbigh J S 1985 *Entropy in Relation to Incomplete Knowledge* (Cambridge: Cambridge University Press)
Derrida B and Flyvbjerg H 1987 *J. Phys. A: Math. Gen.* **20** 5273
Deutscher G, Zallen R and Adler J (ed) 1983 *Percolation structure and processes; Ann. Isr. Phys. Soc.* **5**
Englman R, Jaeger Z and Levi A 1984 *Phil. Mag.* B **50** 307
Englman R, Rivier N and Jaeger Z 1988a *Nucl. Phys.* B (Proc. Suppl.) **5A** 345
—— 1988b *Phil. Mag.* B **56** 751
Esterling D 1979 *Comments Solid State Phys.* **9** 105
Faber K, Iwagoshi T and Ghosh A 1988 *J. Am. Ceram. Soc.* **71** C-399
Glenn L A and Chudnovsky A 1986 *J. Appl. Phys.* **59** 379
Glenn L A, Gommerstadt B Y and Chudnovsky A 1986 *J. Appl. Phys.* **60** 1224
Grady D E 1982 *J. Appl. Phys.* **53** 322
Grady D E, Bergstresser T K and Taylor J M 1985 *Sandia Report No.* 85-1545
Grady D E and Kipp M E 1985 *J. Appl. Phys.* **58** 1210
—— 1989 *Structural Failure* ed T Wierzbicki (New York: Wiley) ch 1
Griffith A A 1920 *Phil. Trans. R. Soc.* A **221** 163
Griffith L 1943 *Can. J. Res.* **21** 57
Gross D H E 1990 *Rep. Prog. Phys.* **53** 605
Hirth J P 1972 *Metall. Trans.* **3** 3047
Irwin G R 1957 *J. Appl. Mech.* **24** 361
Jaeger Z and Englman R 1991 *Trans. ASME* No 1 at press
Jaeger Z, Englman R, Gur Y and Sprecher A 1986a *J. Mater. Sci. Lett.* **5** 5
Jaeger Z, Englman R and Slotky D 1986b *Ann. Isr. Phys. Soc.* **8** 517
Jaeger Z, Englman R and Sprecher A 1986c *J. Appl. Phys.* **59** 40
Jaynes E T 1983 *Papers on Probabilities, Statistics and Statistical Physics* ed R D Rosenkrantz (Dordrecht: Reidel)
—— 1985 *Highly Informative Priors in Bayesian Statistics 2* ed J M Bernard *et al* (New York: Elsevier) pp 329–60
Jeffreys H 1961 *The Theory of Probability* 3rd edn (Oxford: Oxford University Press) ch III
Johnson N L and McKnight D S 1987 *Artificial Space Debris* (FL: Orbit) pp 35 and 73
Jones G E, Kennedy J E and Bertholf L D 1980 *Am. J. Phys.* **48** 264
Kachanov L M 1986 *Introduction to Continuum Damage Mechanics* (Dordrecht: Martinus Nijhoff)
Kaufman J H, Melroy O R and Dimino G M 1989 *Phys. Rev.* A **39** 1420–8
Kessler D J 1985 *Adv. Space Res.* **5** 3
Kiguchi M, Narita S, Miyama S M and Hayashi C 1988 *Prog. Theor. Phys.* (Suppl.) **96** 63
Kikuchi R 1970 *J. Chem. Phys.* **53** 2713
Kipp M E and Grady D E 1985 *J. Mech. Phys. Solids* **33** 399
Kipp M E, Grady D E and Chen E P 1980 *Int. J. Fract.* **16** 471
Kleinert H 1989 *Gauge Field Theories in Condensed Matter* (Singapore: World Scientific)
Knight W D, Clemenger K, De Heer W, Saunders W, Chou M and Cohen M 1984 *Phys. Rev. Lett.* **52** 2141
Kuszmaul J S 1986 *Sandia Report No.* 86-2427C
Latanision R and Pickens J (ed) 1983 *Atomistics of Fracture* (New York: Plenum)
Lefebvre A H 1989 *Atomization and Sprays* (New York: Hemisphere)
Levine R D 1985 *Theory of Chemical Reaction Dynamics* vol 4, ed M Baer (Boca Raton, FL: CRC) p 1
Levinger N E, Ray D, Alexander M L and Lineberger W C 1988 *J. Chem. Phys.* **89** 5654
Lin X, Wei H-Z, Zhu H-S and Yu Q 1989 *Proc. 11th Int. Symp. on Ballistics (Brussels, May 1989)* vol 2, pp 569–75
MacAulay M A 1987 *Introduction to Impact Engineering* (London: Chapman and Hall)
Mai Y W and Lawn B R 1987 *J. Am. Ceram. Soc.* **70** 289
McGrady E D and Ziff M 1987 *Phys. Rev. Lett.* **58** 892
McHugh S 1983 *Proc. Ist Int. Symp. on Rock Fragmentation by Blasting (Lulea, Sweden)* vol 1, ed R Holmberg and A Rustan, pp 407–18
Mock W Jr and Holt W M 1983 *J. Appl. Phys.* **54** 2344
Mott N F 1947 *Proc. R. Soc.* **189** A 300
Mott N F and Linfoot E H 1943 *Ministry of Supply (GB) Report* AC 3348
Narita S, Miyama S M, Kiguchi M and Hayashi C 1988 *Prog. Theor. Phys.* (Suppl.) **96** 50

Paskin A, Som D K and Dienes G J 1983 *Acta Metall.* **31** 1253, 1841
Phillips J C 1986 *Chem. Rev.* **86** 619
Prigogine I 1978 *Science* **201** 777
Raj R and Ashby M F 1975 *Acta Metall.* **23** 653
Rajendran A M and Elfer N 1989 *Structural Failure* ed T Wierzbicki and N Jones (New York: Wiley) p 4
Ravid M and Bodner S R 1983 *Int. J. Eng. Sci.* **21** 577
Ravid M, Bodner S R and Holcman I 1987 *Int. J. Eng. Sci.* **25** 473
Rayane D, Melinon P, Cabaud B, Hoareau A, Tribollet B and Broyer M 1989 *J. Chem. Phys.* **90** 3295
Rice I 1975 *Constitutive Equations in Plasticity* ed A S Argon (Cambridge, MA: MIT Press) p 23
Rivier N, Englman R and Levine R D 1990 *Maximum Entropy and Bayesian Methods* ed P F Fougère (Dordrecht: Kluwer) pp 233–42
Rosenblatt-Roth M 1987 *C.R. Acad. Sci., Paris* **304** 343
—— 1988 *C.R. Acad. Sci., Paris* **306** 283
Seaman L, Gran J and Curran D R 1984 *Application of Fracture Mechanics to Cementitous Composites* ed S P Shah (NATO-ARW, Northwestern University, Evanston, IL)
Sellens R W 1989 *Part. Part. Syst. Charact.* **6** 17
Sellens R W and Brzustowski T A 1986 *Combust. Flame* **65** 273
Shannon C E 1948 *Bell Syst. Technol. J.* **27** 379
Shockey D A, Seaman L and Curran D R 1985 *Int. J. Fracture* **27** 145
Sih G C 1983 *Can. Fracture Conf.* **10** 65
Skilling J 1984 *Nature* **312** 382
—— 1989 *Maximum Entropy and Bayesian Methods* ed J Skilling (Dordrecht: Kluwer) pp 45–62
Stahler S W 1983 *Astrophys. J.* **268** 115
Stauffer D 1979 *Phys. Rep.* **54** 1
—— 1981 *Scaling Properties of Percolation Clusters (Lecture Notes in Physics 149)* (Heidelberg: Springer) pp 9–25
—— 1985 *Introduction to Percolation Theory* (London: Taylor and Francis)
Stephens P W and King J G 1981 *Phys. Rev. Lett.* **51** 1538
Sternberg H M 1973 *NOLTR Report 73-83* (INTIS, Springfield, VA)
Stronge W I, Xiaoing M and Lanting Z 1989 *Int. J. Mech. Sci.* **31** 811
Tate A 1967 *J. Mech. Phys. Solids* **15** 387
—— 1969 *J. Mech. Phys. Solids* **17** 141
Taylor L M, Kuszmaul J S and Chen E P 1985 *ASCE/ASME Mechanics Conf. (Albuquerque, NM, June 1985)* AMD vol 69, p 95
Thomson R 1986 *Physics of Fracture (Solid State Physics 39)* ed H Ehrenreich and D Turnbull (Orlando: Academic) pp 2–129
Thomson R and Fuller E 1982 *Fracture Mechanics in Ceramics* ed R C Bradt, D P H Hasselman and E F Lange (New York: Plenum)
Tikochinsky Y, Tishby N Z and Levine R D 1984 *Phys. Rev. Lett.* **52** 1357
Titterington D M 1984 *Nature* **312** 381
Tuler F R and Butcher B M 1968 *Int. J. Fracture Mech.* **4** 431
Turcotte D L 1986 *J. Geophys. Res.* **91** 1921
Waddington C J and Freier P S 1985 *Phys. Rev.* C **31** 888
Wagner H D and Eitan A 1990 *Appl. Phys. Lett.* **56** 1965
Weiland P, Wien K, Della-Negra S, Depaw J, Joret H and Le Beyec Y 1989 *J. Physique Coll.* **50** C2 141
Weiner R J and Rogers H C 1979 *J. Appl. Phys.* **50** 8025
Yatom H and Ruppin R 1989 *J. Appl. Phys.* **65** 112
Zallen R 1983 *The Physics of Amorphous Solids* (New York: Wiley)
Ziff R M and McGrady E D 1986 *Macromolecules* **19** 2513
Zurek W H 1989 *Phys. Rev.* A **40** 4731